Global trends of carbon sequestration and their link to increasing CO_2 and climate warming

Authors: M. Fernández-Martínez[*1]. J. Sardans[2,3,] F. Chevallier[4], P. Ciais[4], M. Obersteiner[5], S. Vicca[1], J. G. Canadell[6], A. Bastos[4], P. Friedlingstein[7], S. Sitch[7], S.L. Piao[8,9], I.A. Janssens[1], J. Peñuelas[2,3].

Affiliations:

[1] Centre of Excellence PLECO (Plant and Vegetation Ecology), Department of Biology, University of Antwerp, 2610 Wilrijk, Belgium.

[2] CSIC, Global Ecology Unit, CREAF-CSIC-UAB, Cerdanyola del Vallès, 08193 Barcelona, Catalonia, Spain

[3] CREAF, Cerdanyola del Vallès, 08193 Barcelona, Catalonia, Spain

[4] Laboratoire des Sciences du Climat et de l'Environnement, CEA CNRS UVSQ, 91191 Gif-sur-Yvette, France

[5] International Institute for Applied Systems Analysis, Schlossplatz 1, 2361 Laxenburg, Austria

[6] Global Carbon Project, CSIRO Oceans and Atmosphere, Canberra, ACT 2601, Australia

[7] College of Engineering, Computing and Mathematics, University of Exeter, Exeter EX4 4QF, UK

[8]Sino-French Institute of Earth System Sciences, College of Urban and Environmental Sciences, Peking University, Beijing 100871, China

[9] Institute of Tibetan Plateau Research, Chinese Academy of Sciences, Beijing 100085, China

*Correspondence to: M. Fernández-Martínez, marcos.fernandez-martinez@uantwerpen.be

Abstract

Theory and observations indicate that elevated atmospheric CO_2 concentrations increase leaf-scale photosynthesis. However, changes in climate, availability of soil nutrients, and ecosystem structure at canopy and ecosystem scales, can modify the positive effect of increasing CO_2 on net ecosystem production (NEP). Whether increased photosynthesis ultimate drives an increase in NEP depends on the turnover time of carbon in ecosystems. We analysed spatial and temporal variation in NEP derived from global atmospheric-inversion models (MACC-II and Jena CarboScope) and combined these with simulations of the TRENDY dynamic global vegetation multi-model ensemble and statistical models to differentiate between the effects of increasing CO_2 and changing land use and climate. The effects of atmospheric deposition of nitrogen and sulphur on NEP for Europe and the USA were also analysed. We found that the increase in global NEP from 1995 to 2014 was consistent in both inversion models and the TRENDY ensemble. Increasing CO_2 was positively associated with increasing NEP, and increasing temperatures were negatively associated with NEP trends (for MACC-II, Jena CarboScope and TRENDY). The estimated global sensitivities for CO_2 and temperature were 67 ± 1 Tg C ppm^{-1} and -974 ± 232 Tg C $°C^{-1}$ for the MACC-II dataset and 92 ± 4 Tg C ppm^{-1} and -1704 ± 600 Tg C $°C^{-1}$ for the Jena CarboScope dataset, respectively. We also detected that the estimated global sensitivity for CO_2 has decreased during the studied period. The effects of land-use change on NEP differed amongst the datasets. The effects of oxidised nitrogen deposition on NEP differed between the two datasets, but they all indicated that increasing CO_2 has contributed to increases in NEP in Europe and the USA. Our results indicate that CO_2 fertilisation is a driver of a large-scale increase in carbon sinks and that climatic warming is having a negative impact on carbon sinks.

Introduction

Terrestrial ecosystems have been absorbing 15–30% of the anthropogenic CO_2 emissions for decades (Canadell *et al.*, 2007; Le Quéré *et al.*, 2016). Direct and indirect anthropogenic impacts on the biosphere, however, can alter this compensating mechanism in the short and long term (Ciais *et al.*, 2005; Crowther *et al.*, 2016; Fernández-Martínez *et al.*, 2017; Peñuelas *et al.*, 2017). Identifying the factors that affect the capacity of the biosphere to absorb carbon (C) and quantify their effect is of paramount importance for increasing confidence in future projections of the coupled C cycle/climatic system.

The increase in atmospheric CO_2 concentrations is one of the most evident direct impacts of anthropogenic activity (Ciais *et al.*, 2013), and increasing productivity (e.g. photosynthesis) is a common response to increasing atmospheric CO_2 concentrations under controlled experimental conditions (Ainsworth & Long, 2005; Medlyn *et al.*, 2015). The scientific community, however, is still trying to determine if the increases in CO_2 can increase large-scale photosynthesis (the CO_2 fertilisation effect), primary productivity, and the strength of the terrestrial C sink (Keenan *et al.*, 2013; Fernández-Martínez *et al.*, 2017). Assessing the effect of CO_2 on net ecosystemic production (NEP) is of special interest, because non-respired photosynthesised C can, potentially, be sequestered for long periods, thereby buffering the increase in atmospheric CO_2. Detecting the effect of elevated CO_2 on C fluxes, however, is much more difficult than under controlled experiments, because annual variability in C fluxes (gross primary production [GPP], ecosystemic respiration [Re], and NEP) depend on multiple factors. Some recent efforts have been successful using eddy-covariance towers, which have detected positive effects of CO_2 on water-use efficiency (WUE), photosynthesis, and NEP based on statistical models (Keenan *et al.*, 2013; Fernández-Martínez *et al.*, 2017).

At the same time, increasing atmospheric CO_2 concentrations are also responsible for climatic warming (Alexander *et al.*, 2013). The potential positive effect of elevated CO_2 concentrations on productivity could be partly offset by global warming (Peñuelas *et al.*, 2017) and altered precipitation patterns (Alexander *et al.*, 2013); both water availability and temperature are strong drivers of photosynthesis and respiration worldwide (Fernández-Martínez *et al.*, 2014a). Large-scale land-use change can also alter the capacity of the biosphere to sequester C. Atmospheric deposition of nitrogen (N) and sulphur (S) from the use of fossil fuels and N fertilisers may also alter ecosystemic function, productivity and the C balance (Wamelink *et al.*, 2009a, 2009b; de Vries &

Posch, 2011; de Vries *et al.*, 2014; Fernández-Martínez *et al.*, 2017). N deposition is usually positively correlated with ecosystemic productivity and NEP (Magnani *et al.*, 2007; Luyssaert *et al.*, 2010; de Vries *et al.*, 2014) and can enhance the positive effect of CO_2 (Quinn Thomas *et al.*, 2010). Despite of this general trend, several field studies have observed that long-term N loads can reduce plant growth and ecosistemic carbon sink capacity (Granath *et al.*, 2014; Ochoa-Hueso *et al.*, 2017). On the other hand, S deposition seems to have mainly a negative effect (Oulehle *et al.*, 2011; Thomas *et al.*, 2013). Acid rain occurs with high rates of both N and S deposition, which are usually correlated in time and space. Soil acidification, caused by acid deposition, often decreases the availability of soil nutrients (Truog, 1946) and reduces C sequestration and can therefore limit NEP (Fernández-Martínez *et al.*, 2017). Differentiating between the combined effects of increasing CO_2, climate change, and atmospheric deposition on C sequestration requires an analysis of all these variables together and advanced statistical techniques.

These findings, however, were limited mainly to temperate and boreal sites, so whether or not their results are scalable globally is difficult to determine. Extensive spatial and temporal monitoring of the terrestrial C balance is of paramount importance for learning about the plausible biogeochemical processes and drivers of anthropogenic changes that affect the global CO_2 sink. Inversion models, and remotely sensed data (Zhu *et al.*, 2016), can be used to test the generality of the patterns derived from ground-based measurements. Inversion models provide continuous gridded data for the net flux of land-atmosphere CO_2 exchange (i.e. NEP) with global coverage, based on measurements of atmospheric CO_2 concentrations and on an atmospheric-transport model (Rödenbeck *et al.*, 2003; Chevallier *et al.*, 2010). Inversions provide regional details of CO_2 fluxes at typical temporal scales of weeks and at spatial scales of 250-400 km (for the inversions listed above). Small-scale features are more uncertain than fluxes integrated over large latitudinal bands, and in regions with few stations reflect mainly prior flux settings, and are sensitive to errors in transport models. The gridded NEP datasets from inversions, combined with CO_2-concentration records, gridded datasets for climate, land-use change, and atmospheric deposition, allow us to make a first attempt to study the combined effects of CO_2, changes in climate and land use, and atmospheric N and S deposition on terrestrial NEP patterns at the global scale.

We quantified the trends in annual NEP in terrestrial ecosystems for the last two decades (1995–2014) and determined if these changes were statistically associated with increasing atmospheric CO_2 and changing land uses and climate (temperature, precipitation, and drought) at the global scale. We also analysed the effect of changing

rates of atmospheric deposition of oxidised and reduced N and S on NEP, combined with increasing CO_2 and changing climate and land use, over Europe and the United States of America (USA).

Methods

Datasets

NEP data

We used gridded global monthly NEP data for 1995–2014 from two inversion models: i) the MACC (Monitoring Atmospheric Composition and Climate) CO_2 (http://www.gmes-atmosphere.eu/catalogue/)(Chevallier *et al.*, 2005) database, version v14r2 and ii) the Jena-CarboScope database version s93_v3.7 using a constant network of towers. The MACC CO_2 atmospheric inversion system relies on the variational formulation of Bayes' theorem to analyse direct measurements of CO_2 concentrations from 130 sites around the globe for 1979-2014. Optimised fluxes were calculated at a global horizontal resolution of 3.75 × 1.875° (longitude, latitude) and a temporal resolution of eight days, separately for daytime and night-time. The underlying transport model was run with interannually varying meteorological data from the ECMWF ERA-Interim reanalysis. The Jena inversion model estimates the interannual variability of CO_2 fluxes based on raw CO_2 concentration data from 50 sites. The model uses a variational approach with the TM3 transport model (4 × 5°, using interannually varying winds). Prior terrestrial fluxes were obtained from a modelled mean biospheric pattern and fossil-fuel emissions (Rödenbeck *et al.*, 2003). We also used NEP data from an ensemble of 10 dynamic global vegetation models (DGVMs) compiled by the TRENDY project (models CLM4.5, ISAM, JSBACH, JULES, LPJG, LPX, OCN, ORCHIDEE, VEGAS, and VISIT). We used the output from simulation experiment S3, which was run with varying atmospheric CO_2 and changing land use and climate.

Meteorological, land-use change and atmospheric CO_2 data

We extracted gridded temperature and precipitation time series from the Climatic Research Unit TS3.23 dataset (Harris *et al.*, 2013). We also used the SPEI (Standardised Precipitation-Evapotranspiration Index) drought index (Vicente-serrano *et al.*, 2010) from the global SPEI database (http://spei.csic.es/database.html) as a measure of drought intensity (positive values indicate wetter than average meteorological conditions, negative values indicate drier than average conditions). We used annual SPEI1 (monthly SPEI averaged over a year). Mean annual temperature (MAT) and precipitation (MAP) and SPEI were calculated for each year and pixel. We

used land-use change maps from land-use harmonisation[2] (LUH2, http://luh.umd.edu/data.shtml) and calculated the percent coverages of forests, croplands, and urban areas per pixel, so we could further estimate whether they increased or decreased from 1995 to 2014. We used the data for atmospheric CO_2 concentration from Mauna Loa Observatory provided by the Scripps Institution of Oceanography (Scripps CO_2 programme).

Data for N and S deposition

Annual data for N (oxidised N [N_{OX}] from NO_3^- and reduced N [N_{RED}] from NH_4^+) and S (SO_4^-) wet deposition were extracted from: i) the European Monitoring and Evaluation Programme (EMEP) with a spatial resolution of 0.15 × 0.15° for longitude and latitude, ii) the MSC-W chemical-transport model developed to estimate regional atmospheric dispersion and deposition of acidifying and eutrophying N and S compounds over Europe, and iii) the National Atmospheric Deposition Program (NADP) covering the USA with a spatial resolution of 0.027 × 0.027° for longitude and latitude. We used only data for wet deposition because the NADP database only contained records for dry deposition for 2000. Analyses focused on atmospheric deposition and were restricted to Europe and the USA because temporal gridded maps of atmospheric deposition were not available for other regions. Maps of atmospheric deposition for the regional analyses were adjusted to the resolution of the C-flux maps (3.75 × 1.875° for the MACC-II model and 4 × 5° for the Jena CarboScope model for longitude and latitude).

Statistical analyses

To determine how NEP has changed from 1995 to 2014, we first calculated the trends for each pixel in both inversion models and an average dataset of the TRENDY ensemble using linear regressions with an autoregressive and moving-average (ARMA) (p=1, q=0) correlation structure to account for temporal autocorrelation. Trends over larger areas (e.g. the entire world, latitudinal bands), either for NEP or the predictor variables, were calculated using generalised linear mixed models (GLMMs) with random slopes (e.g. NEP ~ year). We used pixel as the random factor (affecting the slopes of the year), and an ARMA (p=1, q=0) correlation structure. All average trends shown were calculated using this methodology.

The temporal contributions of increasing CO_2, climate (MAT, MAP, and SPEI), and land-use change (forests, croplands, and urban areas) to the observed trends in NEP were assessed for the MACC-II, Jena CarboScope, and TRENDY datasets for the entire world. For the MACC-II and Jena CarboScope datasets, we repeated the

analysis for five latitudinal bands to determine if the contributions of CO_2, climate, and land-use change were globally consistent. In addition, to assess if the effects of CO_2 and MAT on NEP were changing with time, we split the datasets in three blocks of 10 years each (1995-2004, 2000-2009 and 2005-2014). After fitting the models, we calculated the temporal contributions of CO_2 and MAT on NEP trends for the three periods considered.

We also determined the temporal contribution of atmospheric deposition of N (N_{OX} and N_{RED}) and S to the trends in NEP in a combined analysis that also included CO_2, climatic, and land-use trends. This latter analysis was restricted to Europe and the USA due to the lack of atmospheric-deposition time series for the rest of the world.

The temporal contributions of the predictor variables were calculated as follows:

i) using a GLMM with an autocorrelation structure for lag 1 (AR1) and using the pixel as the random factor, we fitted full models for NEP as a function of CO_2, mean MAT per pixel, annual anomaly of MAT, mean MAP per pixel, annual anomaly of MAP, the annual SPEI, and mean percentage of forested, cropped, and urban areas per pixel and their annual anomalies. We included the first-order interaction terms between CO_2 and all predictors and between the mean values and the anomalies for all predictors (except SPEI, which interacted with mean MAT and MAP). When the interaction term between the means and the anomalies (e.g. MAT mean × MAT anomaly) was included, the model estimated the effect of the anomaly as a function of the average value. This implies a change in the effect of increasing or decreasing the anomalies, depending on the mean for the site (e.g. increasing temperature may have a positive effect in cold climates but a negative effect in warmer climates). For models including atmospheric deposition, we also included the interaction between climatic variables and CO_2 and the interactions between the means and the annual anomalies of atmospheric deposition (N_{OX}, N_{RED}, and S). The models were fitted using maximum likelihood to allow the comparison of models with different fixed factors.

ii) We used the stepwise backwards-forwards model selection (*stepAIC* function in R) from the full models, using the lowest Bayesian information criterion (BIC), to achieve the final model. The amount of the variance explained by the models was assessed using the *r.squaredGLMM* function in R (MuMIn package: (Barton, 2015)) following the method of Nakagawa and Schielzeth (2013). Model residuals met the assumptions required in all analyses.

iii) We then used the final models to predict the changes of the response variables during the study period (1995–2014). We first extracted the observed trend (mean ± SEM, standard error of the mean) in NEP using raw data with GLMMs with an AR1 autocorrelation structure. We then calculated the trend of NEP predicted by the final model and the trends of NEP predicted by the same model while maintaining the temporally varying predictors constant one at a time (e.g. MAT anomalies were held constant using the median per pixel, while all other predictors changed based on the observations). The difference between the predictions for the final model and when one predictor was controlled was assumed to be the contribution of that predictor variable to the change in NEP. The differences between all individual contributions and the observed trend in NEP were treated as unknown contributions. Finally, we calculated the average sensitivities of NEP to the predictor changes by dividing the temporal contributions of each predictor by their temporal trends. All errors were calculated using the error-propagation method. All analyses were performed for both inversion models (MACC-II and Jena CarboScope).

Results

Global trends in NEP, and the contributions of CO_2 and climate

Both datasets (MACC-II and Jena CarboScope) indicated an overall positive trend in NEP globally from 1995 to 2014. The estimated NEP increased by 0.87 ± 0.05 g C m^{-2} y^{-1} for the MACC-II dataset, by 1.32 ± 0.06 g C m^{-2} y^{-1} for the Jena CarboScope dataset, and by 0.15 ± 0.06 g C m^{-2} y^{-1} for the TRENDY ensemble (**Figure 1**). Both MACC-II and Jena CarboScope datasets produced similar trends for many parts of the world, an increasing NEP for Siberia, Asia, Oceania, and South America, and a decreasing NEP for the southern latitudes of Africa. Nonetheless, considerable differences emerged for Europe and North America. Jena CarboScope indicated primarily positive trends for Europe and primarily negative trends for North America, but MACC II indicated more variation in the trends for both continents. The trends identified by the TRENDY ensemble differed widely from those identified by the MACC-II and Jena CarboScope datasets, except for the northernmost latitudes, for which they all indicated an increasing C-sink capacity.

Our statistical analyses attributed the increases in global NEP to increasing CO_2 but found a consistent negative impact of temperature on NEP, which limited the positive effect of increasing CO_2 (**Figure 1**). These results were consistent for both datasets and most of the DGVMs of the TRENDY ensemble. The sensitivity of NEP to

255 increasing CO_2 averaged 0.45 ± 0.01 and 0.62 ± 0.03 g C m^{-2} ppm^{-1} for the MACC-II
256 and Jena CarboScope models, respectively **(Table 1)**, representing sensitivities over
257 the entire terrestrial surface of 67 ± 1 and 92 ± 4 Tg C ppm^{-1}, respectively. Despite
258 lower temporal attributions for temperature than CO_2, the sensitivity of NEP to
259 temperature was high, at -6.6 ± 1.6 and -11.5 ± 4.0 g C m^{-2} y^{-1} $°C^{-1}$ for the MACC-II and
260 Jena CarboScope models, respectively, equivalent to global sensitivities of -974 ± 232
261 and -1704 ± 600 Tg C $°C^{-1}$, respectively.

262 Further analyses focused on 10-year windows revealed that the positive contribution of
263 CO_2 has consistently decreased in both atmospheric inversion models for the last two
264 decades (**Figure 2a**). However, this decreasing pattern was not shown by the DGVMs
265 of the TRENDY ensemble. Both inversion models and the TRENDY ensemble showed
266 that negative temporal contribution of MAT on NEP also decreased with time (**Figure**
267 **2b**), specially for the last 10 years of our study. Global MAT decreased 0.24 ± 0.02 ºC
268 during this last 10-year period in the meteorological data used here.

269 Other predictor variables explained significant spatial and temporal variation in NEP,
270 even though only CO_2 and annual temperature contributed consistently and
271 significantly to the observed trends in NEP in the MACC-II, Jena CarboScope, and
272 TRENDY datasets. Our statistical analyses for the MACC-II and Jena CarboScope
273 datasets indicated that the positive effect of CO_2 on NEP was higher in regions with
274 higher annual precipitation and that this positive effect increased with temperature
275 (**Figure 3, Supplementary Information 1.1**). Increasing temperatures, though,
276 reduced NEP in warm regions but increased in cold regions. SPEI (negative values
277 indicate drought) had a slightly negative effect on NEP in regions with low MAP but had
278 a positive effect in wet regions (**Figure 3**).

279 The same analyses performed for inversion NEP averaged over latitudinal bands
280 (boreal, >55°; temperate, 35-55°; subtropical, 15-35°; and tropical, 15°N-15°S) further
281 supported the previous results obtained at the global scale (**Figure 4, Supplementary**
282 **Information 1.2–1.7**). Increasing CO_2 was the main factor accounting for increasing
283 trends in NEP, with a consistent positive temporal contribution for all latitudinal bands
284 considered and for both datasets (except for MACC-II at northern subtropical latitudes
285 and Jena CarboScope at northern boreal latitudes). Increasing temperatures had a
286 consistent negative effect for all latitudinal bands, but most effects were not significant.
287 Increasing temperatures, however, had a stronger negative effect on NEP for the
288 tropical bands, where temperatures were higher, as found by the global analysis
289 (**Figure 3**). Estimated NEP sensitivities to CO_2 and temperature even differed by an

290 order of magnitude between the datasets and latitudinal bands but were consistent with
291 the previous results indicating a positive effect of increasing CO_2 and a negative effect
292 of increasing temperatures (**Table 1**).

293 *Analyses of atmospheric deposition over Europe and the USA*

294 The MACC-II and Jena CarboScope datasets indicated that NEP increased over
295 Europe and the USA by 0.45 ± 0.13 and 0.68 ± 0.16 g C m^{-2} y^{-1}, respectively (**Figure**
296 **5**). Our statistical models again indicated that increasing atmospheric CO_2 in both
297 datasets contributed significantly to increasing NEP. NEP sensitivity to CO_2 was more
298 than two-fold higher in the Jena CarboScope than the MACC-II dataset (**Table 2**),
299 similar to the temporal contributions, at 0.19 ± 0.06 and 0.50 ± 0.07 g C m^{-2} y^{-1} ppm^{-1}
300 for the MACC-II and Jena CarboScope models, respectively. The temporal contribution
301 of decreasing N_{OX} deposition to NEP differed between the two datasets; the
302 contribution was positive for MACC-II and negative for Jena CarboScope. Our analyses
303 consequently estimated a negative sensitivity of NEP to N_{OX} for the MACC-II dataset
304 but a positive sensitivity for the Jena CarboScope dataset. Additionally, the analyses
305 for effects of land-use change (for forested and cropped areas) yielded contrasting
306 results for both datasets, but neither MACC-II, nor Jena CarboScope indicated a strong
307 impact of land use change. Despite being significant predictors in our statistical models
308 (**Supplementary Information 1.8**), the changes in N_{RED}, S_{OX}, MAT, MAP, and
309 urbanised area did not significantly contribute to the trends in continental NEP but
310 presented significant temporal trends (except MAP).

311 Our analyses for both datasets indicated that the positive effect of CO_2 on NEP was
312 higher in regions with higher N_{RED} deposition but lower in regions with high S deposition
313 (means for MACC-II and annual anomalies for Jena CarboScope; see **Supplementary**
314 **Information 1.8**). The results for N_{OX} deposition, however, differed between the
315 models. The positive effect of CO_2 on NEP for the MACC-II dataset was constrained by
316 the annual anomalies of N_{OX} but was higher for the Jena CarboScope dataset. These
317 discrepancies were also evident in the estimated average effects of N_{OX} and S, for both
318 mean per pixel and annual anomalies. Our statistical model for the MACC-II dataset
319 estimated positive average effects of mean and annual anomalies for N_{OX}, but the
320 average effect of N_{OX} anomalies was negative for the Jena CarboScope dataset. The
321 MACC-II dataset indicated an average positive effect of mean S deposition per site and
322 an average negative effect of its anomalies. The Jena CarboScope dataset produced
323 opposite results.

324 **Discussion**

Our global results for the MACC-II, Jena CarboScope, and TRENDY ensemble datasets, with long-term time series of NEP, indicated that NEP increased globally from 1995 to 2014. Increasing atmospheric CO_2 was the main factor associated with this global positive trend, albeit its effect decreased with time. These results were consistent for all latitudinal bands and even when climate and atmospheric deposition were used as additional drivers of changes in NEP. Climatic warming consistently reduced global NEP, which suggests that terrestrial sinks will become increasingly more vulnerable to continuous global warming in the future (Peñuelas *et al.*, 2017), thereby decreasing their capacity to store C for long periods. The global contribution of land-use change to trends in NEP was not consistent amongst the datasets, neither globally nor using latitudinal bands. The reduction of S deposition did not significantly contribute to the NEP trends, and the effect of N_{OX} on the NEP trends remained elusive because the results from the MACC-II and Jena CarboScope datasets did not agree. N_{RED}, though, did not change significantly during this period, so it could not contribute to the trends in NEP. The results for the MACC-II and Jena CarboScope datasets, however, demonstrated that the effect of CO_2 fertilisation was stronger in regions with higher rates of N_{RED} deposition.

Effect of CO_2 fertilisation on global NEP

NEP is determined by a combination of processes that counteract each other (e.g. photosynthesis, autotrophic respiration [Ra], and heterotrophic respiration [Rh]). The positive effect of atmospheric CO_2 on NEP must thus be due to a mechanistic effect on these processes. Increasing atmospheric CO_2 concentrations have been widely reported to increase ecosystemic photosynthesis, mainly by two mechanisms: i) by increasing carboxylation rates and decreasing photorespiration (Aber *et al.*, 2001), and ii) by decreasing stomatal conductance and therefore increasing WUE (Prentice *et al.*, 2000; Keenan *et al.*, 2013), which would theoretically increase photosynthesis under water limitation. An increase in GPP by either mechanism may thus account for the higher NEP due to increasing atmospheric CO_2, with a recent global analysis suggesting that most of the GPP gains are due to increased ecosystemic WUE (Cheng *et al.*, 2017). The increase in atmospheric CO_2, however, should thus stimulate Re less than GPP, as recently suggested using eddy-covariance towers (Fernández-Martínez *et al.*, 2017).

Increasing atmospheric CO_2 may also have contributed to a decrease in Re without a change in GPP, perhaps due to an increased C:N ratio of litter (Sardans *et al.*, 2012), which may decrease Rh (Norby *et al.*, 2001; Wu *et al.*, 2001) and therefore potentially

increase C-sink capacity. However, microbial activity may also increase under elevated CO_2, for example as a consequence of increased root exudation (Bengtson *et al.*, 2012). This mechanism could counteract the positive effect of increasing the C:N ratio of litter. In summary, the increase in NEP is most likely due to the stimulation of photosynthesis, at a constant or only slightly higher Re.

Our estimates of global NEP sensitivity to CO_2 were 0.45 ± 0.02 and 0.62 ± 0.05 g C m^{-2} ppm^{-1} (globally 67 ± 1 and 92 ± 4 Tg C ppm^{-1}) for the MACC-II and Jena CarboScope datasets, respectively, but the estimates varied amongst the latitudinal bands and were inconsistent between datasets (**Table 2**). These estimates were similar to those reported in CO_2-enrichment FACE experiments (Norby *et al.*, 2010) but lower than those reported in a study using eddy-covariance flux towers for a similar period (Fernández-Martínez *et al.*, 2017). The much larger areas analysed by the inverse models than the footprints covered by the eddy-covariance flux towers may have contributed to the differences between the estimates. Towers are usually located in relatively homogenous ecosystems, but each pixel in inverse models aggregates information from several ecosystems (and even biomes), often including non-productive land such as bare soil or cities. Estimates are therefore understandably lower from inverse models than from eddy-covariance flux towers.

Our results indicated that the variability of the estimates of NEP sensitivity to CO_2 amongst the latitudinal bands might be associated with differences in climate and atmospheric deposition. The two atmospheric inversion models indicated that the effect of CO_2 fertilisation was stronger in wet climates (high annual precipitation) (**Figure 3**), supporting the estimates provided by the latitudinal bands, with the highest sensitivity estimates for the tropical band (**Table 2**). The positive effect of CO_2 tended to increase with temperature, even though increasing temperatures had a negative impact on NEP, and this effect was higher in warmer regions (**Figures 1-4, Supplementary Information 1.1–1.7**). Both the MACC-II and Jena CarboScope datasets, however, indicated a stronger positive effect of increasing CO_2 in regions with higher N_{RED} deposition, which agrees with other studies suggesting that the effect of CO_2 fertilisation is stronger in nitrogen-rich sites (Van Groenigen *et al.*, 2006; Terrer *et al.*, 2017). Despite the general positive effect of CO_2 on NEP, we detected a decrease on its effect during the last two decades of this study (**Figure 2a**), further supporting the evidence of previous studies suggesting that the positive effect of increasing CO_2 on increasing ecosystem productivity and carbon sink capacity may be saturating (Peñuelas *et al.*, 2017). Our results also suggest that the DGVMs of the TRENDY ensemble need to improve to be able to capture this decreasing effect of CO_2 on NEP.

Longer time series will be necessary to confirm whether the effect of CO_2 fertilisation on NEP will continue to increase with temperature or will eventually saturate and subsequently decrease, as suggested here, due to other limiting factors such as nutrient availability and their imbalances or changes in rates of atmospheric deposition (Raupach *et al.*, 2007; Peñuelas *et al.*, 2013; Fernández-Martínez *et al.*, 2014b).

Climate and land-use changes and C sinks

Climatic warming clearly had a secondary effect on the trends in NEP from 1995 to 2014. The MACC-II and Jena CarboScope datasets estimated that NEP decreased globally by around -974 ± 232 and -1704 ± 600 Tg C for every degree of increase in Earth's temperature. However, we also found that the negative temporal contribution of MAT on NEP trends has decreased for the last two decades (**Figure 2b**). These results, consistent using both atmospheric inversions and the TRENDY ensemble, may be link to the average global MAT decrease of 0.24 ± 0.02 ºC, during the last 10 years of the study in the meteorological data used here, conversely to the monotonic increase in CO_2 concentrations.

Atmospheric CO_2 concentrations have been more important than increasing temperatures for NEP trends, although recent evidence suggests a shift in importance of the two opposing forces driving C sequestration worldwide: the positive effect of CO_2 fertilisation and the overall negative effect of increasing temperature (Peñuelas *et al.*, 2017). Our results are nonetheless consistent to those of a recent similar analysis using remotely sensed data (Zhu *et al.*, 2016) and eddy-covariance towers, in which the changing climate during the last 20 years did not significantly contribute to changing C fluxes in 23 temperate and boreal forests in Europe and the USA (Fernández-Martínez *et al.*, 2017). Our results clearly indicate a small negative effect of increasing temperatures on NEP, which may have been impossible to detect with a shorter and smaller dataset, demonstrating the necessity to explore these types of relationships with datasets comprising both large areas and long periods.

Increasing temperature, however, did not have the same effect on NEP around the world. The analyses for both inverse models indicated that increasing temperatures have had a positive effect on NEP only in very cold regions (MAT of -20 °C) (**Figure 3**). This general negative effect of temperature on NEP could be due to a greater stimulation of Ra than photosynthesis by higher temperatures (Ryan, 1991; Amthor, 1994). The potential benefit to C sequestration of increased photosynthesis would then be negated by a higher increase in Re. Increasing temperatures can also be linked to drier conditions, which may decrease GPP more than Re (Wu *et al.*, 2011).

Changing conditions of drought and precipitation did not have a significant effect on NEP trends, despite accounting for the interannual variability in NEP. Our statistical models indicated that, on average, NEP was higher in wet years in wet regions and tended to be lower in wet years in dry regions (**Figure 3**). This interaction between precipitation and drought could be due to constraints on decomposition and thus respiration by the low humidity in dry regions (MAP <300 mm y^{-1}) (e.g. in Mediterranean soils, see Jarvis et al. [2007]). Decomposition in these regions would increase during wet years, releasing C to the atmosphere and decreasing NEP.

The effects of land-use change on the NEP trends, though, differed greatly amongst the datasets, both at the global scale or using latitudinal bands. An analysis with a resolution as coarse as ours could blur the effect of land-use change on the NEP trends until it became undetectable. Our statistical models, however, identified significant relationships for land-use change, but the large differences in effects amongst the datasets preclude drawing firm conclusions.

Atmospheric deposition and the terrestrial C balance

The effects of N_{OX} deposition were divergent in both the MACC-II and Jena CarboScope datasets for temporal and spatial variability. Conclusions about the effect of N_{OX} on regional NEP thus cannot be drawn from our analyses. The discrepancy in the results for N_{OX} in **Figure 5** and **Table 2** was due to the different NEP trends for Europe and the USA for both models. Conversely, the trends in NEP were very similar for the rest of the world, which provided very consistent global and latitudinal results for the effect of increasing CO_2 and temperature. N_{RED} did not significantly contribute to the trends in NEP for either of the inversion models (**Figure 5),** mainly because it did not have a significant trend over time. N_{RED}, however, was a good predictor of spatial and interannual NEP variability (see **Supplementary Information 1.8**), in contrast to N_{OX}. Analysing the deposition of oxidised and reduced N separately rather than only using the total amount of N, as has been done so far (Magnani *et al.*, 2007; Janssens *et al.*, 2010; de Vries & Posch, 2011; Fernández-Martínez *et al.*, 2014a), may thus lead to a better understanding of the effect of N deposition. S deposition did not significantly contribute to the trends in NEP, which contrasts with a recent study using eddy-covariance towers (Fernández-Martínez *et al.*, 2017). The lack of an effect of S in this case could be due to the local scale of its effects, which would be lost when analysing larger geographical scales. The large spatial heterogeneity of soil properties, such as pH, could also play a role obfuscating the effects of S deposition when using data with such a coarse resolution. Additionally, the different sign of the estimates for S in our

statistical models indicated inconsistency amongst the datasets, which further indicated that conclusions for the effects of S deposition on large-scale NEP cannot be drawn from our analyses.

Conclusions

Our analyses underscored the dominant role of the effect of CO_2 fertilisation on vegetation growth in driving the global terrestrial C sink between 1995 and 2014. We also identified a consistent and offsetting negative effect of warming on terrestrial sinks at the global scale, suggesting an increase in the vulnerability of the terrestrial sinks to continued increases in global temperatures. Additionally, the positive effect of increasing CO_2 on global C sink capacity seems to be decreasing, jeopardizing the future capacity of the biosphere to mitigate global warming. This new body of knowledge highlights the multi-factorial nature of earth-system dynamics controlling excess atmospheric CO_2, and ultimately anthropogenic climate change, and calls for the development of integrative approaches that can fully exploit the growing wealth of observations and understanding of processes.

Acknowledgements

This research was supported by the European Research Council Synergy grant ERC-2013-726 SyG-610028 IMBALANCE-P, the Spanish Government project CGL2016-79835-P (FERTWARM), and the Catalan Government project SGR 2014-274. M.F.M. was funded by a postdoctoral subsidy from the University of Antwerp. S.V. is a postdoctoral fellow of the Research Foundation – Flanders (FWO). J.G.C. thanks the support of the National Environmental Science Programme ESCC Hub.

References:

Aber J, Neilson RP, McNulty S, Lenihan JM, Bachelet D, Drapek RJ (2001) Forest Processes and Global Environmental Change: Predicting the Effects of Individual and Multiple Stressors. *BioScience*, **51**, 735.

Ainsworth EA, Long SP (2005) What have we learned from 15 years of free-air CO2 enrichment (FACE)? A meta-analytic review of the responses of photosynthesis, canopy properties and plant production to rising CO2. *The New phytologist*, **165**, 351–71.

Alexander L, Allen S, Bindoff NL et al. (2013) *Climate Change 2013: The Physical Science Basis - Summary for Policymakers*. Intergovernmental Panel on Climate Change.

Amthor JS (1994) Scaling CO2 Photosynthesis Relationships from the Leaf to the Canopy. *Photosynthesis Research*, **39**, 321–350.

Barton K (2015) MuMIn: Multi-model inference. R package version 1.17.1. http://CRAN.R-project.org/package=MuMIn.

Bengtson P, Barker J, Grayston SJ (2012) Evidence of a strong coupling between root exudation, C and N availability, and stimulated SOM decomposition caused by rhizosphere priming effects. *Ecology and evolution*, **2**, 1843–52.

Canadell JG, Le Quéré C, Raupach MR et al. (2007) Contributions to accelerating atmospheric CO2 growth from economic activity, carbon intensity, and efficiency of natural sinks. *Proceedings of the National Academy of Sciences of the United States of America*, **104**, 18866–70.

Cheng L, Zhang L, Wang Y-P et al. (2017) Recent increases in terrestrial carbon uptake at little cost to the water cycle. *Nature Communications*, **8**, 110.

Chevallier F, Fisher M, Peylin P et al. (2005) Inferring CO 2 sources and sinks from satellite observations: Method and application to TOVS data. *Journal of Geophysical Research*, **110**, D24309.

Chevallier F, Ciais P, Conway TJ et al. (2010) CO 2 surface fluxes at grid point scale estimated from a global 21 year reanalysis of atmospheric measurements. *Journal of Geophysical Research*, **115**, D21307.

Ciais P, Reichstein M, Viovy N et al. (2005) Europe-wide reduction in primary productivity caused by the heat and drought in 2003. *Nature*, **437**, 529–533.

Ciais P, Sabine C, Bala G et al. (2013) The physical science basis. Contribution of working group I to the fifth assessment report of the intergovernmental panel on climate change. *Change, IPCC Climate*, 465–570.

Crowther TW, Todd-Brown KEO, Rowe CW et al. (2016) Quantifying global soil carbon losses in response to warming. *Nature*, **540**, 104–108.

Fernández-Martínez M, Vicca S, Janssens IA et al. (2014a) Spatial variability and controls over biomass stocks, carbon fluxes and resource-use efficiencies in forest

529 ecosystems. *Trees, structure and function*, **28**, 597–611.

530 Fernández-Martínez M, Vicca S, Janssens IA et al. (2014b) Nutrient availability as the
531 key regulator of global forest carbon balance. *Nature Climate Change*, **4**, 471–
532 476.

533 Fernández-Martínez M, Vicca S, Janssens IA et al. (2017) Atmospheric deposition,
534 CO2, and change in the land carbon sink. *Scientific Reports*, **7:9632**, 1–13.

535 Granath G, Limpens J, Posch M, Mücher S, De Vries W (2014) Spatio-temporal trends
536 of nitrogen deposition and climate effects on Sphagnum productivity in European
537 peatlands. *Environmental Pollution*, **187**, 73–80.

538 Van Groenigen KJ, De Graaff MA, Six J, Harris D, Kuikman P, Van Kessel C (2006)
539 The Impact of Elevated Atmospheric CO2 on Soil C and N Dynamics. *Ecological*
540 *Studies*, **187**, 374–391.

541 Harris I, Jones PDD, Osborn TJJ, Lister DHH (2013) Updated high-resolution grids of
542 monthly climatic observations - the CRU TS3.10 Dataset. *International Journal of*
543 *Climatology*, **34**, online, update.

544 Janssens I a., Dieleman W, Luyssaert S et al. (2010) Reduction of forest soil
545 respiration in response to nitrogen deposition. *Nature Geoscience*, **3**, 315–322.

546 Jarvis P, Rey A, Petsikos C et al. (2007) Drying and wetting of Mediterranean soils
547 stimulates decomposition and carbon dioxide emission: the “Birch effect.” *Tree*
548 *Physiology*, **27**, 929–940.

549 Keenan TF, Hollinger DY, Bohrer G, Dragoni D, Munger JW, Schmid HP, Richardson
550 AD (2013) Increase in forest water-use efficiency as atmospheric carbon dioxide
551 concentrations rise. *Nature*, **499**, 324–327.

552 Luyssaert S, Ciais P, Piao SL et al. (2010) The European carbon balance. Part 3:
553 forests. *Global Change Biology*, **16**, 1429–1450.

554 Magnani F, Mencuccini M, Borghetti M et al. (2007) The human footprint in the carbon
555 cycle of temperate and boreal forests. *Nature*, **447**, 848–50.

556 Medlyn BE, Zaehle S, De Kauwe MG et al. (2015) Using ecosystem experiments to
557 improve vegetation models. *Nature Climate Change*, **5**, 528–534.

558 Nakagawa S, Schielzeth H (2013) A general and simple method for obtaining R 2 from

559 generalized linear mixed-effects models (ed O'Hara RB). *Methods in Ecology and*
560 *Evolution*, **4**, 133–142.

561 Norby RJ, Cotrufo MF, Ineson P, O'Neill EG, Canadell JG (2001) Elevated CO2, litter
562 chemistry, and decomposition: a synthesis. *Oecologia*, **127**, 153–65.

563 Norby RJ, Warren JM, Iversen CM, Medlyn BE, McMurtrie RE (2010) CO2
564 enhancement of forest productivity constrained by limited nitrogen availability.
565 *Proceedings of the National Academy of Sciences of the United States of*
566 *America*, **107**, 19368–73.

567 Ochoa-Hueso R, Munzi S, Alonso R et al. (2017) Ecological impacts of atmospheric
568 pollution and interactions with climate change in terrestrial ecosystems of the
569 Mediterranean Basin: Current research and future directions. *Environmental*
570 *Pollution*, **227**, 194–206.

571 Oulehle F, Evans CD, Hofmeister J et al. (2011) Major changes in forest carbon and
572 nitrogen cycling caused by declining sulphur deposition. *Global Change Biology*,
573 **17**, 3115–3129.

574 Peñuelas J, Poulter B, Sardans J et al. (2013) Human-induced nitrogen-phosphorus
575 imbalances alter natural and managed ecosystems across the globe. *Nature*
576 *communications*, **4**, 2934.

577 Peñuelas J, Ciais P, Canadell JG et al. (2017) Shifting from a fertilization-dominated to
578 a warming dominated period. *Nature Ecology and Evolution*, **1**, 1438–1445.

579 Prentice IC, Heimann M, Sitch S (2000) The carbon balance of the terrestrial
580 biosphere: Ecosystem models and Atmospheric observations. *Ecological*
581 *Applications*, **10**, 1553–1573.

582 Le Quéré C, Andrew RM, Canadell JG et al. (2016) Global Carbon Budget 2016. *Earth*
583 *System Science Data*, **8**, 605–649.

584 Quinn Thomas R, Canham CD, Weathers KC, Goodale CL (2010) Increased tree
585 carbon storage in response to nitrogen deposition in the US. *Nature Geoscience*,
586 **3**, 13–17.

587 Raupach MR, Marland G, Ciais P, Le Quéré C, Canadell JG, Klepper G, Field CB
588 (2007) Global and regional drivers of accelerating CO2 emissions. *Proceedings of*
589 *the National Academy of Sciences of the United States of America*, **104**, 10288–

590 93.

591 Rödenbeck C, Houweling S, Gloor M, Heimann M (2003) CO_2 flux history 1982–2001
592 inferred from atmospheric data using a global inversion of atmospheric transport.
593 *Atmospheric Chemistry and Physics*, **3**, 1919–1964.

594 Ryan MG (1991) Effects of climate change on plant respiration. *Ecological*
595 *Applications*, **1**, 157–167.

596 Sardans J, Rivas-Ubach A, Peñuelas J (2012) The C:N:P stoichiometry of organisms
597 and ecosystems in a changing world: A review and perspectives. *Perspectives in*
598 *Plant Ecology, Evolution and Systematics*, **14**, 33–47.

599 Terrer C, Vicca S, Hungate BA et al. (2017) Response to Comment on "Mycorrhizal
600 association as a primary control of the CO_2 fertilization effect." *Science*, **355**,
601 358.3-358.

602 Thomas RB, Spal SE, Smith KR, Nippert JB (2013) Evidence of recovery of Juniperus
603 virginiana trees from sulfur pollution after the Clean Air Act. *Proceedings of the*
604 *National Academy of Sciences of the United States of America*, **110**, 15319–24.

605 Truog E (1946) Soil Reaction Influence on Availability of Plant Nutrients1. *Soil Science*
606 *Society of America Journal*, **11**, 305.

607 Vicente-serrano SM, Beguería S, López-Moreno JI (2010) A Multiscalar Drought Index
608 Sensitive to Global Warming: The Standardized Precipitation Evapotranspiration
609 Index. *Journal of Climate*, **23**, 1696–1718.

610 de Vries W, Posch M (2011) Modelling the impact of nitrogen deposition, climate
611 change and nutrient limitations on tree carbon sequestration in Europe for the
612 period 1900–2050. *Environmental Pollution*, **159**, 2289–2299.

613 de Vries W, Du E, Butterbach-Bahl K (2014) Short and long-term impacts of nitrogen
614 deposition on carbon sequestration by forest ecosystems. *Current Opinion in*
615 *Environmental Sustainability*, **9**–**10**, 90–104.

616 Wamelink GWW, Wieggers HJJ, Reinds GJ, Kros J, Mol-Dijkstra JP, van Oijen M, De
617 Vries W (2009a) Modelling impacts of changes in carbon dioxide concentration,
618 climate and nitrogen deposition on carbon sequestration by European forests and
619 forest soils. *Forest Ecology and Management*, **258**, 1794–1805.

620 Wamelink GWW, van Dobben HF, Mol-Dijkstra JP, Schouwenberg EP a. G, Kros J, De

621 Vries W, Berendse F (2009b) Effect of nitrogen deposition reduction on
622 biodiversity and carbon sequestration. *Forest Ecology and Management*, **258**,
623 1774–1779.

624 Wu H, Hayes MJ, Weiss A, Hu Q (2001) An evaluation of the Standardized
625 Precipitation Index, the China-Z Index and the statistical Z-Score. *International*
626 *Journal of Climatology*, **21**, 745–758.

627 Wu Z, Dijkstra P, Koch GW, Peñuelas J, Hungate B a. (2011) Responses of terrestrial
628 ecosystems to temperature and precipitation change: a meta-analysis of
629 experimental manipulation. *Global Change Biology*, **17**, 927–942.

630 Zhu Z, Piao S, Myneni RB et al. (2016) Greening of the Earth and its drivers. *Nature*
631 *Climate Change*, **6**, 791–795.

632

Figure 1: Global trends in NEP for the a) MACC-II, b) Jena CarboScope, and c) TRENDY ensemble datasets. The temporal contributions of CO_2 and climate to the observed trends in NEP are shown on the right side of each panel. The difference between the modelled contributions and the observed trends (shaded) has been treated as an unknown contribution to the temporal variation in NEP. Statistically significant ($P < 0.05$) temporal variations of the predictors are shown in square brackets. Error bars indicate 95% confidence intervals. The boxplots in panel c indicate the estimated contributions of the 10 DVGMs used in the TRENDY ensemble. Units are ppm y^{-1} for CO_2, °C y^{-1} for temperature, mm y^{-2} for precipitation, standard deviation for SPEI, and percentage of land-use cover per pixel for forests, crops, and urban areas. See the Materials and Methods section for information about the methodology used to calculate the contributions. Significance levels: *, $P < 0.05$; **, $P < 0.01$; ***, $P < 0.001$.

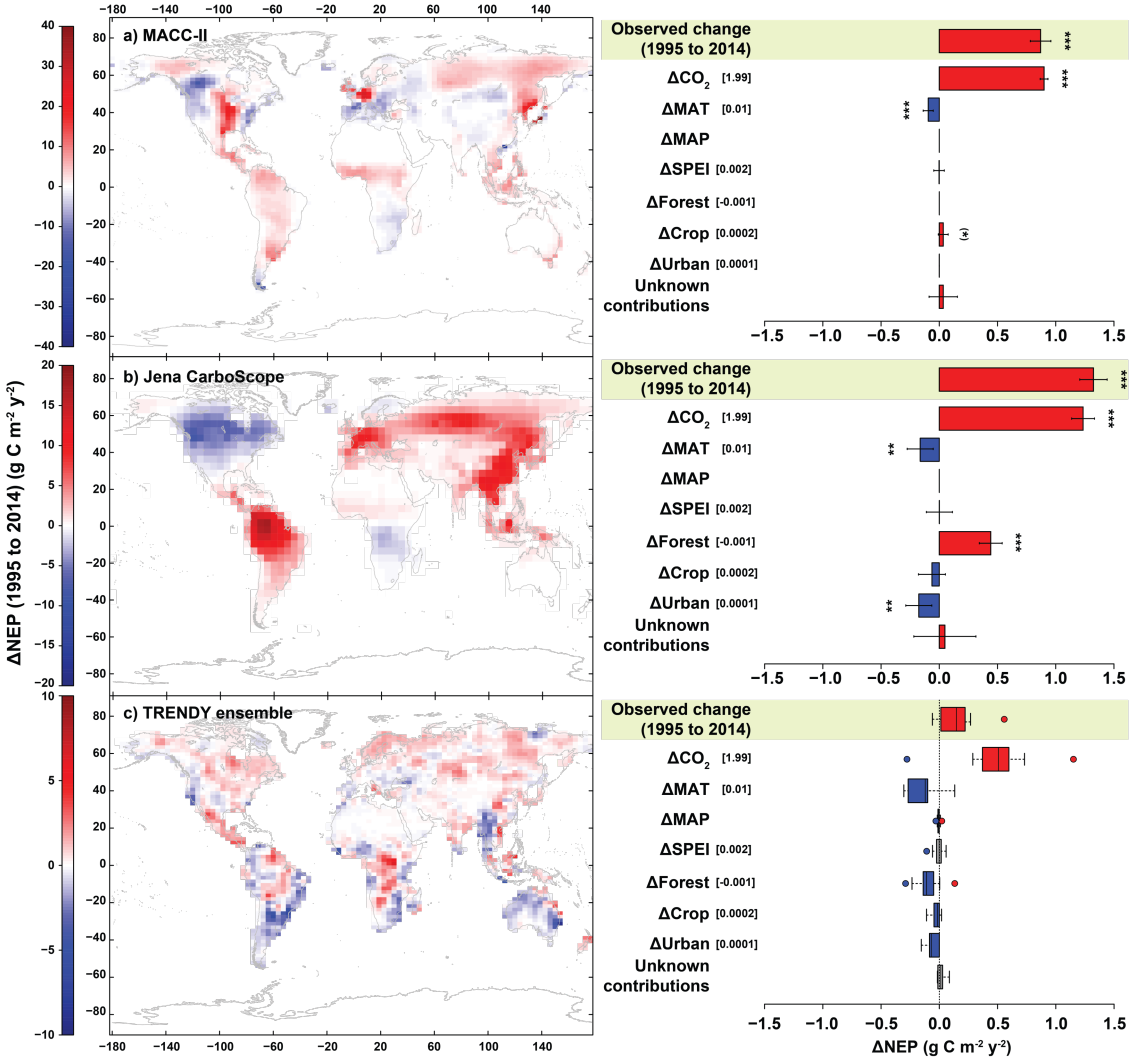

Figure 2: Evolution of the temporal contribution of a) atmospheric CO_2 concentrations and b) MAT on NEP according to MACC-II, Jena CarboScope, and TRENDY ensemble datasets for the last two decades. Error bars indicate the 95% confidence intervals of the estimates.

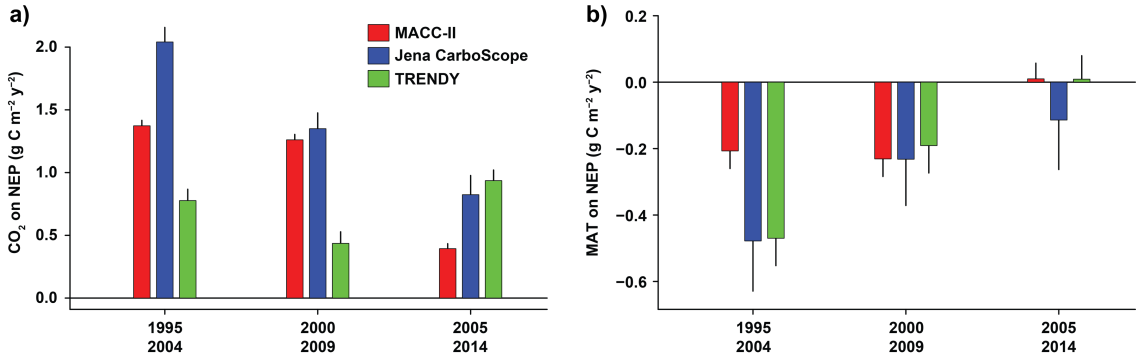

Figure 3: Plots showing the estimated effects of the interactions between CO_2 and climate (mean annual precipitation [MAP] and temperature [MAT], annual anomalies in temperature [MAT.an], and the Standardised Precipitation-Evapotranspiration Index [SPEI]) on NEP for the MACC-II and Jena CarboScope inversion models. Shaded bands indicate the 95% confidence intervals of the slopes. Vertical lines at the bottoms of the plots indicate data distributions for the x-axes.

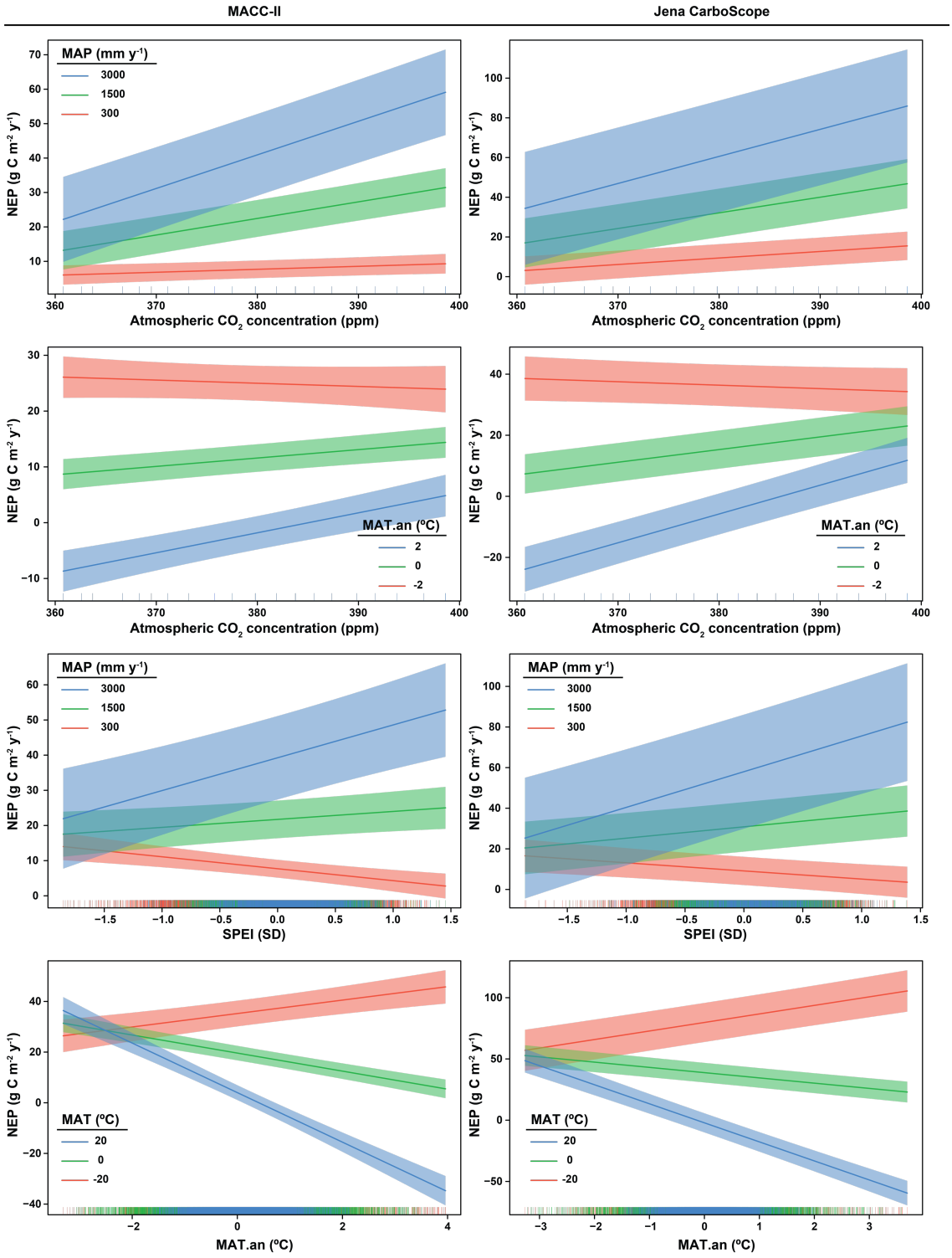

Figure 4: Latitudinal trends in NEP for the MACC-II and Jena CarboScope datasets. The difference between the modelled contributions and the observed trends (shaded) has been treated as an unknown contribution to the temporal variation in NEP. Only statistically significant ($P < 0.05$) trend contributors are shown. Statistically significant temporal variations of the predictors are shown in square brackets. Error bars indicate 95% confidence intervals. Units are ppm y^{-1} for CO_2, °C y^{-1} for temperature, mm y^{-2} for precipitation, standard deviation for SPEI, and percent cover for forests, crops, and urban areas. See the Materials and Methods section for information about the methods used to calculate the contributions. Significance levels: *, $P < 0.05$; **, $P < 0.01$; ***, $P < 0.001$.

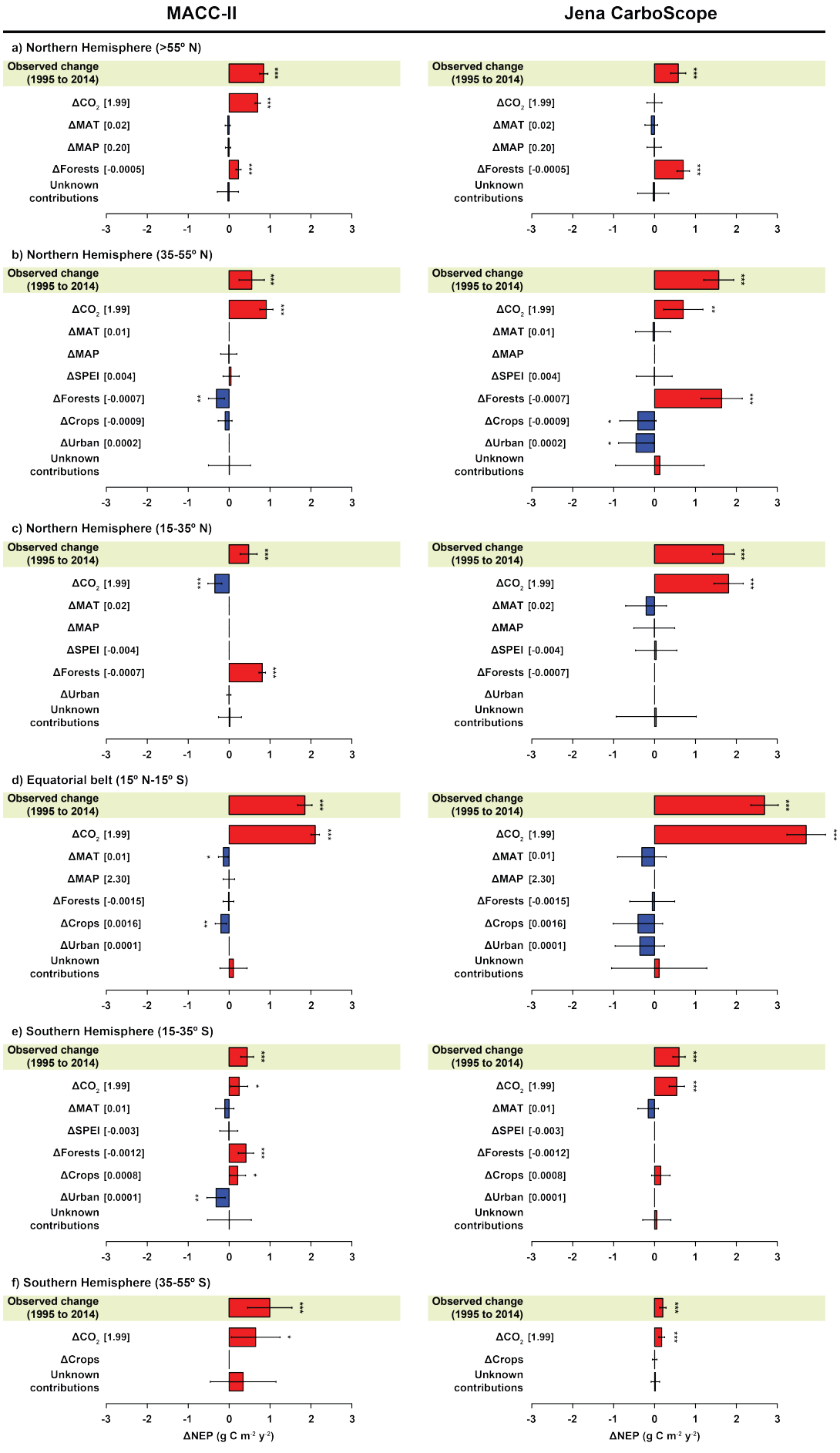
MACC-II
Jena CarboScope
a) Northern Hemisphere (>55° N)
b) Northern Hemisphere (35-55° N)
c) Northern Hemisphere (15-35° N)
d) Equatorial belt (15° N-15° S)
e) Southern Hemisphere (15-35° S)
f) Southern Hemisphere (35-55° S)
Observed change (1995 to 2014)
ΔCO2 [1.99]
ΔMAT [0.02]
ΔMAP [0.20]
ΔForests [-0.0005]
Unknown contributions
ΔMAT [0.01]
ΔMAP
ΔSPEI [0.004]
ΔForests [-0.0007]
ΔCrops [-0.0009]
ΔUrban [0.0002]
ΔSPEI [-0.004]
ΔUrban
ΔMAP [2.30]
ΔForests [-0.0015]
ΔCrops [0.0016]
ΔUrban [0.0001]
ΔSPEI [-0.003]
ΔForests [-0.0012]
ΔCrops [0.0008]
-3 -2 -1 0 1 2 3
ΔNEP (g C m-2 y-2)

Figure 5: Temporal contributions of the predictor variables to changes in NEP for the MACC-II and Jena CarboScope inversion models. The SPEI drought index does not appear in the table because it was not a significant predictor in either of the models. Units are g C m^{-2} y^{-1}. Error bars indicate 95% confidence intervals. Significance levels: $^{(*)}$, $P < 0.10$; *, $P < 0.05$; **, $P < 0.01$; ***, $P < 0.001$.

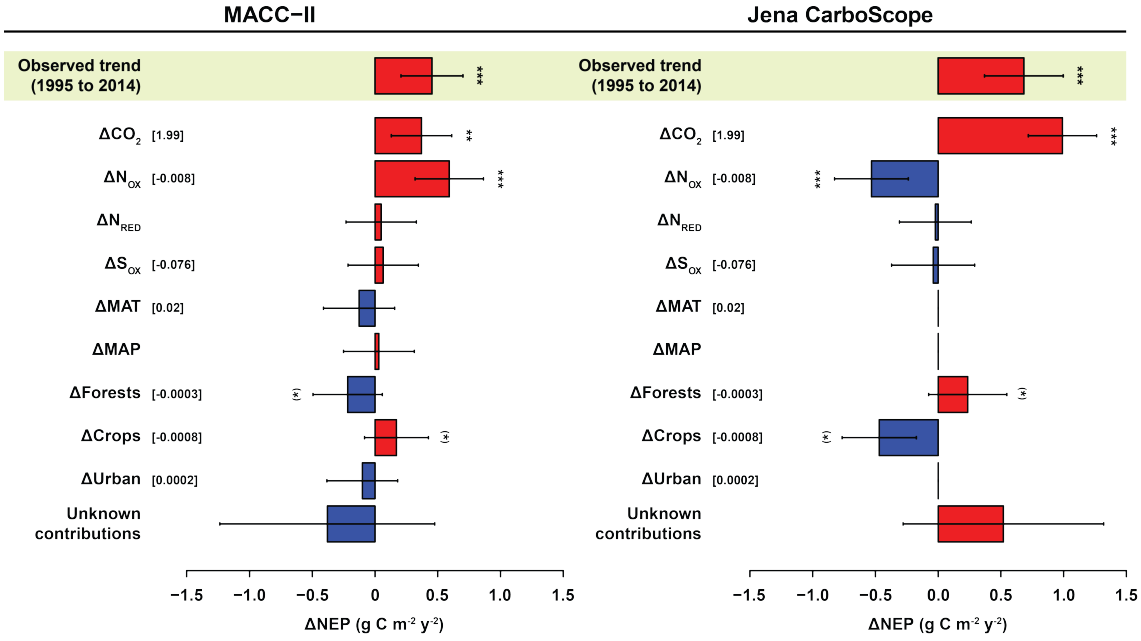

678 **Table 1:** Global and latitudinal analyses of sensitivity of NEP to changes in
679 atmospheric CO_2 concentrations and mean annual temperature. Units are g C m^{-2} y^{-1}
680 ppm^{-1} for CO_2 and g C m^{-2} y^{-1} C^{-1} for temperature. NH and SH indicate Northern and
681 Southern Hemispheres, respectively. Boreal analyses comprise latitudes >55°,
682 temperate latitudes from 35 to 55°, subtropical latitudes from 15 to 35°, and tropical
683 latitudes from 15°S to 15°N. Bold coefficients differ significantly from 0 at the 0.05 level.

	Dataset	CO_2	Temperature
Global	**MACC-II**	**0.45 ± 0.01**	**-6.57 ± 1.57**
	Jena CarboScope	**0.62 ± 0.03**	**-11.49 ± 4.04**
NH Boreal	**MACC-II**	**0.35 ± 0.02**	-1.60 ± 1.59
	Jena CarboScope	0.00 ± 0.05	-3.77 ± 3.77
NH Temperate	**MACC-II**	**0.46 ± 0.04**	
	Jena CarboScope	**0.35 ± 0.12**	-3.32 ± 19.89
NH Subtropical	**MACC-II**	**-0.18 ± 0.04**	
	Jena CarboScope	**0.91 ± 0.09**	-12.17 **±** 15.07
Tropical	**MACC-II**	**1.06 ± 0.03**	**-14.96 ± 6.52**
	Jena CarboScope	**1.86 ± 0.12**	-35.21 ± 34.74
SH Subtropical	**MACC-II**	**0.12 ± 0.05**	-12.96 ± 14.10
	Jena CarboScope	**0.27 ± 0.05**	-16.79 ± 14.15
SH Temperate	**MACC-II**	**0.33 ± 0.15**	
	Jena CarboScope	**0.09 ± 0.02**	

684

685 **Table 2:** Sensitivity of NEP to the predictor variables, including atmospheric deposition
686 for Europe and the USA, for the MACC-II and Jena CarboScope inversion models. The
687 SPEI drought index does not appear in the table because it was not a significant
688 predictor in the models. Units are ppm for CO_2; kg ha^{-1} for N_{OX}, N_{RED}, and S; °C for
689 MAT; mm for MAP, and percentage of land-use cover per pixel for forests, crops, and
690 urban areas. Statistically significant estimates are highlighted in bold.

	MACC-II		**Jena CarboScope**	
	Estimate	***P***	**Estimate**	***P***
CO_2	**0.19 ± 0.06**	**0.0022**	**0.50 ± 0.07**	**0.0000**
N_{OX}	**-72.92 ± 19.92**	**0.0003**	**45.77 ± 14.75**	**0.0017**
N_{RED}	105.20 ± 388.97	0.3943	14.56 ± 95.11	0.4396
S	-0.86 ± 1.89	0.3261	0.45 ± 1.94	0.4085
MAT	-5.80 ± 6.63	0.1931	-	
MAP	-0.21 ± 1.01	0.4166	-	
Forests	676.00 ± 441.93	0.0669	-557.92 ± 396.90	0.0766
Crops	-212.31 ± 162.87	0.0998	536.07 ± 184.09	0.0029
Urban	-544.66 ± 775.27	0.2431	-	

691

Supplementary Information

1. Summary of the models predicting interannual variability in NEP (1995–2014)

Abbreviations: cdioxide, atmospheric CO_2 concentration; MAP.c, climatic mean annual precipitation; MAP.an, interannual deviation from the mean in annual precipitation; MAT.c, climatic mean annual temperature; MAT.an, interannual deviation from the mean in annual temperature; SPEI, Standardised Precipitation-Evapotranspiration Index. R^2_m is the variance explained by a fixed factor, and R^2_c is the total variance explained by the model (fixed + random factors).

1.1 Global model

MACC-II (R^2_m=0.09; R^2_c=0.49)

	Value	SE	Beta	SE	DF	*t*	*P*
(Intercept)	10.327	15.284	0.000	0.000	54249	0.676	0.4992
cdioxide	-0.026	0.040	-0.004	0.007	54249	-0.646	0.5185
MAP.c	-0.096	0.015	-1.000	0.157	2851	-6.370	<0.0001
MAT.an	-42.817	10.134	-0.409	0.097	54249	-4.225	<0.0001
MAT.c	2.915	0.747	0.622	0.159	2851	3.903	0.0001
SPEI	-4.808	1.005	-0.023	0.005	54249	-4.784	<0.0001
Forests.mean	-107.703	33.297	-0.455	0.141	2851	-3.235	0.0012
Urban.mean	247.379	61.835	0.054	0.013	54249	4.001	0.0001
Crops.mean	-716.980	66.998	-1.442	0.135	54249	-10.701	<0.0001
Crops.an	4201.199	810.568	0.662	0.128	54249	5.183	<0.0001
cdioxide:MAP.c	0.000	0.000	1.308	0.153	54249	8.576	<0.0001
cdioxide:MAT.an	0.104	0.027	0.376	0.097	54249	3.876	0.0001
cdioxide:MAT.c	-0.007	0.002	-0.599	0.158	54249	-3.778	0.0002
MAT.an:MAT.c	-0.311	0.027	-0.038	0.003	54249	-11.618	<0.0001
MAP.c:MAT.c	-0.002	0.000	-0.504	0.043	2851	-11.676	<0.0001
MAP.c:SPEI	0.005	0.001	0.023	0.004	54249	5.182	<0.0001
cdioxide:Forests.mean	0.341	0.087	0.546	0.140	54249	3.900	0.0001
cdioxide:Crops.mean	2.088	0.176	1.592	0.134	54249	11.873	<0.0001
cdioxide:Crops.an	-9.983	2.115	-0.601	0.127	54249	-4.719	<0.0001
Crops.mean:Crops.an	-1025.090	152.098	-0.057	0.009	54249	-6.740	<0.0001

Jena CarboScope (R^2_m=0.11; R^2_c=0.82)

	Value	SE	Beta	SE	DF	*t*	*P*
(Intercept)	25.498	19.623	0.000	0.000	21266	1.299	0.1938
cdioxide	-0.035	0.049	-0.004	0.006	21266	-0.701	0.4834
MAP.c	-0.102	0.021	-0.809	0.165	1114	-4.899	<0.0001
MAT.an	-104.263	13.603	-0.711	0.093	21266	-7.665	<0.0001
MAT.c	-6.089	1.048	-0.886	0.152	1114	-5.809	<0.0001
SPEI	-6.400	1.352	-0.023	0.005	21266	-4.733	<0.0001
Forests.mean	-16.085	10.123	-0.051	0.032	1114	-1.589	0.1124
Forests.an	229.501	72.638	0.025	0.008	21266	3.160	0.0016
Urban.an	-1550.128	229.968	-0.027	0.004	21266	-6.741	<0.0001
Crops.mean	-550.600	89.552	-0.805	0.131	1114	-6.148	<0.0001
Crops.an	-434.362	66.417	-0.054	0.008	21266	-6.540	<0.0001
cdioxide:MAP.c	0.000	0.000	1.157	0.147	21266	7.860	<0.0001
cdioxide:MAT.an	0.264	0.036	0.683	0.093	21266	7.352	<0.0001
cdioxide:MAT.c	0.014	0.003	0.769	0.146	21266	5.254	<0.0001
MAT.an:MAT.c	-0.563	0.037	-0.046	0.003	21266	-15.370	<0.0001
MAP.c:MAT.c	-0.002	0.000	-0.491	0.086	1114	-5.679	<0.0001
MAP.c:SPEI	0.008	0.001	0.031	0.004	21266	6.952	<0.0001
Forests.mean:Forests.an	-1703.192	174.638	-0.075	0.008	21266	-9.753	<0.0001
cdioxide:Crops.mean	1.729	0.231	0.959	0.128	21266	7.486	<0.0001
Crops.mean:Crops.an	1117.081	204.895	0.044	0.008	21266	5.452	<0.0001

1.2 Northern Hemisphere, latitudes >55°

MACC-II (R^2_m=0.22; R^2_c=0.60)

	Value	SE	DF	*t*	*P*
(Intercept)	145.378	26.576	17147	5.470	<0.0001
cdioxide	-0.211	0.068	17147	-3.091	0.0020
MAP.an	-0.082	0.010	17147	-8.608	<0.0001
MAP.c	-0.040	0.007	897	-6.085	<0.0001
MAT.an	-4.971	0.500	17147	-9.937	<0.0001
MAT.c	17.628	1.679	897	10.498	<0.0001
Forests.mean	-241.270	34.165	897	-7.062	<0.0001
Forests.an	7804.592	1984.754	17147	3.932	0.0001
Crops.mean	234.696	29.177	897	8.044	<0.0001
MAP.an:MAP.c	0.000	0.000	17147	6.266	<0.0001
cdioxide:MAT.c	-0.036	0.004	17147	-8.246	<0.0001
MAT.an:MAT.c	-0.428	0.048	17147	-8.929	<0.0001
MAP.c:MAT.c	-0.004	0.001	897	-6.487	<0.0001
cdioxide:Forests.mean	0.653	0.089	17147	7.302	<0.0001
cdioxide:Forests.an	-27.703	5.166	17147	-5.362	<0.0001
Forests.mean:Forests.an	3893.244	358.128	17147	10.871	<0.0001

Jena CarboScope (R^2_m=0.31; R^2_c=0.76)

	Value	SE	DF	*t*	*P*
(Intercept)	-120.046	40.956	6487	-2.931	0.0034
cdioxide	0.521	0.104	6487	5.017	<0.0001
MAP.an	0.566	0.130	6487	4.348	<0.0001
MAP.c	0.144	0.057	336	2.528	0.0119
MAT.an	-88.437	9.649	6487	-9.165	<0.0001
MAT.c	4.800	0.697	336	6.889	<0.0001
Forests.mean	211.698	59.662	336	3.548	0.0004
Forests.an	20056.156	2801.938	6487	7.158	<0.0001
Crops.mean	178.659	42.086	336	4.245	<0.0001
cdioxide:MAP.an	-0.002	0.000	6487	-4.381	<0.0001
cdioxide:MAP.c	0.000	0.000	6487	-3.176	0.0015
cdioxide:MAT.an	0.227	0.026	6487	8.901	<0.0001
MAT.an:MAT.c	-0.225	0.049	6487	-4.597	<0.0001
MAP.c:MAT.c	-0.005	0.001	336	-3.875	0.0001
cdioxide:Forests.mean	-0.661	0.156	6487	-4.241	<0.0001
cdioxide:Forests.an	-62.524	7.300	6487	-8.565	<0.0001
Forests.mean:Forests.an	4608.015	548.519	6487	8.401	<0.0001

1.3 Northern Hemisphere, latitudes between 35 and 55°

MACC-II (R^2_m=0.13; R^2_c=0.37)

	Value	SE	DF	*t*	*P*
(Intercept)	118.669	75.095	12204	1.580	0.1141
cdioxide	-0.383	0.197	12204	-1.940	0.0524
MAP.an	-0.054	0.013	12204	-4.231	<0.0001
MAP.c	-0.349	0.079	638	-4.431	<0.0001
MAT.c	21.798	6.08	638	3.585	0.0004
SPEI	-6.661	3.984	12204	-1.672	0.0946
Forests.an	-16174.3	4141.532	12204	-3.905	0.0001
Urban.mean	588.731	97.8	12204	6.020	<0.0001
Crops.mean	-877.546	230.649	638	-3.805	0.0002
Crops.an	1289.549	226.408	12204	5.696	<0.0001
cdioxide:MAP.c	0.001	0	12204	5.675	<0.0001
cdioxide:MAT.c	-0.053	0.016	12204	-3.348	0.0008
MAP.c:MAT.c	-0.009	0.001	638	-7.748	<0.0001
MAP.c:SPEI	0.024	0.007	12204	3.548	0.0004
MAT.c:SPEI	1.177	0.358	12204	3.283	0.0010
cdioxide:Forests.an	43.86	10.904	12204	4.022	0.0001
cdioxide:Crops.mean	2.682	0.608	12204	4.412	<0.0001
Crops.mean:Crops.an	-3213.76	499.299	12204	-6.437	<0.0001

Jena CarboScope (R^2_m=0.11; R^2_c=0.74)

	Value	SE	DF	*t*	*P*
(Intercept)	-322.884	89.772	4394	-3.597	0.0003
cdioxide	1.147	0.234	4394	4.900	<0.0001
MAP.c	-0.319	0.093	226	-3.416	0.0008
MAT.an	-128.427	33.183	4394	-3.870	0.0001
MAT.c	28.759	7.703	226	3.733	0.0002
SPEI	-9.448	3.825	4394	-2.470	0.0135
Forests.mean	2942.176	259.590	226	11.334	<0.0001
Forests.an	-2079.869	229.295	4394	-9.071	<0.0001
Urban.mean	782.381	246.609	226	3.173	0.0017
Urban.an	-2598.987	585.956	4394	-4.435	<0.0001
Crops.mean	-1301.176	271.861	226	-4.786	<0.0001
Crops.an	-12033.683	2911.032	4394	-4.134	<0.0001
cdioxide:MAP.c	0.001	0.000	4394	3.209	0.0013
cdioxide:MAT.an	0.336	0.088	4394	3.827	0.0001
cdioxide:MAT.c	-0.090	0.020	4394	-4.469	<0.0001
MAT.c:SPEI	1.554	0.425	4394	3.655	0.0003
cdioxide:Forests.mean	-7.886	0.679	4394	-11.609	<0.0001
cdioxide:Crops.mean	3.524	0.711	4394	4.959	<0.0001
cdioxide:Crops.an	30.128	7.671	4394	3.928	0.0001
Crops.mean:Crops.an	2875.740	572.620	4394	5.022	<0.0001

1.4 Northern Hemisphere, latitudes between 15 and 35°

MACC-II (R^2_m=0.10; R^2_c=0.48)

	Value	SE	DF	*t*	*P*
(Intercept)	-80.357	30.470	8354	-2.637	0.0084
cdioxide	0.046	0.071	8354	0.641	0.5214
MAP.c	-0.068	0.040	435	-1.695	0.0908
MAT.c	2.617	0.593	435	4.415	<0.0001
Forests.mean	2119.900	425.029	435	4.988	<0.0001
Forests.an	418.904	225.959	8354	1.854	0.0638
Crops.an	-715.190	92.483	8354	-7.733	<0.0001
cdioxide:MAP.c	0.000	0.000	8354	5.305	<0.0001
MAP.c:MAT.c	-0.006	0.001	435	-7.248	<0.0001
cdioxide:Forests.mean	-5.498	1.121	8354	-4.905	<0.0001
Forests.mean:Forests.an	-3820.044	777.773	8354	-4.912	<0.0001

Jena CarboScope (R^2_m=0.40; R^2_c=0.88)

	Value	SE	DF	*t*	*P*
(Intercept)	-53.854	48.278	3394	-1.116	0.2647
cdioxide	0.051	0.081	3394	0.625	0.5318
MAP.an	0.378	0.136	3394	2.777	0.0055
MAP.c	0.143	0.047	173	3.063	0.0025
MAT.an	-12.170	1.797	3394	-6.774	<0.0001
MAT.c	1.393	1.538	173	0.906	0.3661
SPEI	-9.864	3.046	3394	-3.238	0.0012
Forests.mean	-1995.224	122.187	173	-16.329	<0.0001
Crops.mean	-548.606	135.468	173	-4.050	0.0001
cdioxide:MAP.an	-0.001	0.000	3394	-2.868	0.0042
MAP.c:MAT.c	-0.007	0.002	173	-3.716	0.0003
cdioxide:Forests.mean	6.000	0.306	3394	19.604	<0.0001
cdioxide:Crops.mean	1.762	0.345	3394	5.108	<0.0001

1.5 Equatorial belt, latitudes between 15°S and 15°N

MACC-II (R^2_m=0.15; R^2_c=0.48)

	Value	SE	DF	*t*	*P*
(Intercept)	99.812	50.127	9754	1.991	0.0465
cdioxide	0.324	0.090	9754	3.587	0.0003
MAP.an	-0.258	0.064	9754	-4.015	0.0001
MAP.c	-0.139	0.030	508	-4.570	<0.0001
MAT.an	-359.835	58.534	9754	-6.147	<0.0001
MAT.c	-8.327	1.415	508	-5.885	<0.0001
Forests.mean	-537.985	107.454	508	-5.007	<0.0001
Forests.an	6401.221	1527.965	9754	4.189	<0.0001
Crops.mean	-1442.739	190.778	508	-7.562	<0.0001
Crops.an	12801.123	1288.696	9754	9.933	<0.0001
cdioxide:MAP.an	0.001	0.000	9754	4.023	0.0001
cdioxide:MAT.an	0.880	0.155	9754	5.670	<0.0001
MAP.c:MAT.c	0.006	0.001	508	4.685	<0.0001
cdioxide:Forests.mean	1.216	0.283	9754	4.301	<0.0001
cdioxide:Forests.an	-15.978	4.014	9754	-3.981	0.0001
Forests.mean:Forests.an	-856.468	271.383	9754	-3.156	0.0016
cdioxide:Crops.mean	3.885	0.501	9754	7.749	<0.0001
cdioxide:Crops.an	-33.794	3.373	9754	-10.018	<0.0001

Jena CarboScope (R^2_m=0.07; R^2_c=0.78)

	Value	SE	DF	*t*	*P*
(Intercept)	-265.945	61.856	4056	-4.299	<0.0001
cdioxide	0.668	0.159	4056	4.199	<0.0001
MAT.an	-638.717	113.744	4056	-5.615	<0.0001
Forests.mean	-1639.697	184.309	211	-8.896	<0.0001
Forests.an	947.567	165.492	4056	5.726	<0.0001
Urban.an	-4005.091	1352.376	4056	-2.962	0.0031
Crops.mean	-70.948	60.846	211	-1.166	0.2449
Crops.an	9079.254	1969.692	4056	4.609	<0.0001
cdioxide:MAT.an	1.569	0.302	4056	5.199	<0.0001
cdioxide:Forests.mean	4.199	0.480	4056	8.746	<0.0001
Forests.mean:Forests.an	-2350.414	460.905	4056	-5.100	<0.0001
cdioxide:Crops.an	-25.626	5.120	4056	-5.005	<0.0001
Crops.mean:Crops.an	2229.089	499.080	4056	4.466	<0.0001

1.6 Southern Hemisphere, latitudes between 15 and 35°

MACC-II (R^2_m=0.09; R^2_c=0.58)

	Value	SE	DF	*t*	*P*
(Intercept)	-253.810	81.886	5081	-3.100	0.0019
cdioxide	0.690	0.211	5081	3.286	0.0010
MAP.c	-0.110	0.031	262	-3.426	0.0007
MAT.an	-7.850	1.222	5081	-6.420	<0.0001
MAT.c	12.450	3.804	262	3.274	0.0012
SPEI	-2.580	2.498	5081	-1.031	0.3025
Forests.mean	-635.930	192.529	262	-3.303	0.0011
Forests.an	-806.180	86.223	5081	-9.350	<0.0001
Urban.mean	747.840	315.466	262	2.371	0.0185
Urban.an	-4470.740	682.837	5081	-6.547	<0.0001
Crops.an	287.300	41.023	5081	7.003	<0.0001
cdioxide:MAT.c	-0.030	0.010	5081	-3.336	0.0009
MAP.c:MAT.c	0.000	0.001	262	3.520	0.0005
MAP.c:SPEI	0.010	0.003	5081	3.468	0.0005
cdioxide:Forests.mean	1.690	0.504	5081	3.360	0.0008
Forests.mean:Forests.an	2291.060	392.128	5081	5.843	<0.0001
Urban.mean:Urban.an	78460.050	14835.057	5081	5.289	<0.0001

Jena CarboScope (R^2_m=0.15; R^2_c=0.95)

	Value	SE	DF	*t*	*P*
(Intercept)	-14.481	19.009	2066	-0.762	0.4463
cdioxide	0.051	0.041	2066	1.229	0.2192
MAT.an	-158.705	38.384	2066	-4.135	<0.0001
Forests.mean	-1093.533	123.851	106	-8.829	<0.0001
Crops.mean	-383.977	89.994	106	-4.267	<0.0001
Crops.an	209.847	34.031	2066	6.166	<0.0001
cdioxide:MAT.an	0.389	0.102	2066	3.835	0.0001
cdioxide:Forests.mean	2.840	0.282	2066	10.061	<0.0001

1.7 Southern Hemisphere, latitudes between 35 and 55°

MACC-II (R^2_m=0.18; R^2_c=0.31)

	Value	SE	DF	*t*	*P*
(Intercept)	879.820	176.790	1660	4.977	<0.0001
cdioxide	-2.330	0.470	1660	-5.000	<0.0001
MAT.c	-69.030	15.410	84	-4.479	<0.0001
SPEI	-27.680	8.450	1660	-3.278	0.0011
Forests.mean	113.310	23.380	84	4.847	<0.0001
Forests.an	-11891.610	2678.140	1660	-4.440	<0.0001
Urban.mean	403.310	196.790	1660	2.050	0.0406
Urban.an	-5443.000	2154.770	1660	-2.526	0.0116
Crops.mean	-1649.260	448.410	84	-3.678	0.0004
Crops.an	-171.540	150.720	1660	-1.138	0.2552
cdioxide:MAT.c	0.180	0.040	1660	4.538	<0.0001
MAT.c:SPEI	3.080	0.750	1660	4.122	<0.0001
cdioxide:Forests.an	30.520	6.980	1660	4.372	<0.0001
Urban.mean:Urban.an	111819.360	40813.740	1660	2.740	0.0062
cdioxide:Crops.mean	4.310	1.180	1660	3.645	0.0003
Crops.mean:Crops.an	1309.440	439.160	1660	2.982	0.0029

Jena CarboScope (R^2_m=0.003; R^2_c=0.95)

	Value	SE	DF	*t*	*P*
(Intercept)	-39.683	8.216	834	-4.830	<0.0001
cdioxide	0.097	0.019	834	5.180	<0.0001
Crops.an	68.632	11.319	834	6.063	<0.0001

1.8 Europe and the USA (analyses of atmospheric deposition)

Additional abbreviations: N_{OX}.mean, oxidised nitrogen deposition averaged per pixel; N_{OX}.an, N_{OX} interannual deviation from the mean; N_{RED}.mean, reduced nitrogen deposition averaged per pixel; N_{RED}.an, N_{RED} interannual deviation from the mean; S.mean, mean S deposition per pixel; and S.an, S interannual deviation from the mean.

MACC-II (R^2_m=0.22; R^2_c=0.49)

	Value	SE	Beta	SE	DF	*t*	*P*
(Intercept)	-39.577	35.831	0.000	0.000	12634	-1.105	0.2694
cdioxide	0.046	0.094	0.006	0.013	12634	0.493	0.6221
N_{OX}.mean	31.633	6.251	0.436	0.086	656	5.060	<0.0001
N_{OX}.an	566.505	84.592	2.188	0.327	12634	6.697	<0.0001
N_{RED}.mean	-297.072	28.791	-4.854	0.470	656	-10.318	<0.0001
N_{RED}.an	14.861	2.525	0.053	0.009	12634	5.886	<0.0001
S.mean	190.847	15.818	5.552	0.460	656	12.065	<0.0001
S.an	-0.328	1.148	-0.004	0.014	12634	-0.285	0.7753
MAP.an	-0.575	0.173	-0.657	0.198	12634	-3.326	0.0009
MAP.c	-0.009	0.008	-0.038	0.034	656	-1.133	0.2575
MAT.an	-107.714	24.137	-0.864	0.194	12634	-4.463	<0.0001
MAT.c	0.437	0.254	0.064	0.037	656	1.718	0.0862
Forests.mean	53.102	9.381	0.143	0.025	656	5.661	<0.0001
Forests.an	-16680.269	4975.405	-0.936	0.279	12634	-3.353	0.0008
Urban.mean	295.707	90.659	0.090	0.028	12634	3.262	0.0011
Urban.an	423.710	612.950	0.012	0.017	12634	0.691	0.4894
Crops.mean	-4.579	16.349	-0.009	0.034	656	-0.280	0.7795
Crops.an	1116.854	159.565	0.150	0.021	12634	6.999	<0.0001
cdioxide:N_{OX}.an	-1.559	0.226	-2.279	0.330	12634	-6.907	<0.0001
cdioxide:N_{RED}.mean	0.830	0.075	5.145	0.466	12634	11.035	<0.0001
cdioxide:S.mean	-0.458	0.041	-5.057	0.455	12634	-11.123	<0.0001
N_{OX}.an:S.an	4.099	1.204	0.035	0.010	12634	3.404	0.0007
N_{OX}.mean:S.mean	-7.398	0.883	-0.722	0.086	656	-8.379	<0.0001
cdioxide:MAP.an	0.002	0.000	0.654	0.197	12634	3.319	0.0009
cdioxide:MAT.an	0.269	0.064	0.817	0.194	12634	4.221	<0.0001
MAP.c:MAT.c	-0.005	0.000	-0.414	0.045	656	-9.206	<0.0001
cdioxide:Forests.an	49.943	13.062	1.067	0.279	12634	3.824	0.0001
Forests.mean:Forests.an	-4337.808	706.682	-0.110	0.018	12634	-6.138	<0.0001
Urban.mean:Urban.an	-17837.804	5515.859	-0.050	0.016	12634	-3.234	0.0012
Crops.mean:Crops.an	-3572.563	350.836	-0.209	0.021	12634	-10.183	<0.0001

751 **Jena CarboScope (R^2_m=0.33; R^2_c=0.72)**

	Value	SE	Beta	SE	DF	*t*	*P*
(Intercept)	138.920	57.045	0.000	0.000	4545	2.435	0.0149
cdioxide	-0.226	0.149	-0.030	0.020	4545	-1.520	0.1286
N_{OX}.mean	36.244	11.007	0.452	0.137	233	3.293	0.0011
N_{OX}.an	-773.333	140.080	-2.799	0.507	4545	-5.521	<0.0001
N_{RED}.mean	-280.031	36.002	-4.191	0.539	233	-7.778	<0.0001
N_{RED}.an	411.742	119.248	1.323	0.383	4545	3.453	0.0006
S.mean	-83.057	21.414	-2.003	0.516	233	-3.879	0.0001
S.an	213.947	47.142	2.254	0.497	4545	4.538	<0.0001
MAP.c	0.263	0.080	1.213	0.370	233	3.275	0.0012
MAT.c	-1.344	0.453	-0.129	0.043	233	-2.969	0.0033
Forests.an	29318.654	5781.784	1.795	0.354	4545	5.071	<0.0001
Crops.mean	-90.034	30.427	-0.175	0.059	233	-2.959	0.0034
Crops.an	562.020	85.049	0.077	0.012	4545	6.608	<0.0001
cdioxide:N_{OX}.an	2.071	0.376	2.839	0.515	4545	5.514	<0.0001
cdioxide:N_{RED}.mean	0.820	0.093	4.656	0.526	4545	8.847	<0.0001
cdioxide:N_{RED}.an	-1.106	0.314	-1.346	0.382	4545	-3.526	0.0004
cdioxide:S.mean	0.176	0.056	1.607	0.512	4545	3.141	0.0017
cdioxide:S.an	-0.562	0.127	-2.233	0.504	4545	-4.430	<0.0001
N_{OX}.an:N_{RED}.an	43.559	6.267	0.072	0.010	4545	6.951	<0.0001
N_{RED}.an:S.an	-10.807	3.074	-0.051	0.015	4545	-3.515	0.0004
cdioxide:MAP.c	-0.001	0.000	-1.457	0.368	4545	-3.962	0.0001
cdioxide:Forests.an	-78.638	15.263	-1.820	0.353	4545	-5.152	<0.0001

752